**REVISION 2**

# Alkali influence on the water speciation and the environment of protons in silicate glasses revealed by $^{1}$H MAS NMR spectroscopy

Charles Le Losq[1,*], George D. Cody[1], Bjorn O. Mysen[1]

[1]: *Geophysical Laboratory, Carnegie Institution of Washington, 5251 Broad Branch Road NW, Washington D.C. 20015, U.S.A.*

[*]*Corresponding author: clelosq@carnegiescience.edu*

**Keywords**: silicate glasses, proton environment, NMR spectroscopy

**Abstract**

Water can form different chemical bonds with the ionic entities composing silicate melts. Because of that, its influence on the physico-chemical properties of magmas can vary with silicate composition and water content, temperature, and pressure. To further our understanding of how silicate chemical composition governs proton distribution in magmas, the environment of protons in hydrous alkali (Li, Na, K) silicate glasses was varied as a function of the type of alkali metal and total water content. From $^{1}$H MAS NMR spectroscopy, $H^{+}$ are distributed among five different structural environments in alkali silicate glasses. One of these environments is in the form of $H_2O$ molecules ($H_2O_{mol}$). The four others are the proton environments associated with Si-OH bonding, and perhaps also with M-OH bonding (with M = Li, Na or K). Those environments differ in their O-O distance and extent of hydrogen bonding. $H_2O_{mol}$ species are located in an environment with an O-O distance of ~290 pm. $OH^{-}$ groups are in environments with O-O distances from 240 to 305 pm. The ionic

radius of the alkalis, and hence their ionic field strength, determines the fraction of water dissolved as $H_2O_{mol}$ and $OH^-$ groups, as well as the distribution of protons in the various $OH^-$ environments. The mean volume of the $H^+$ oxygen coordination sphere was calculated using the $^1H^+$ NMR signal intensity and the mean O-O distance around $H^+$. Increasing ionic radius of the alkali metal in silicate glasses results in a decrease of this mean volume. The partial molar volume of water in the corresponding melts determined through other technics seems to vary in a comparable way. Therefore, the chemical composition of silicate melts may control the partial molar volume of dissolved water because of its influence on the structural environment of protons. This probably also plays a role in determining water solubility.

## Introduction

Water plays a fundamental role in the dynamics of the past and present Earth because of its major impact on the physicochemical properties of silicate materials. As the main volatile component in natural magmas, water profoundly decreases their viscosity (Richet et al., 1996) so that, for instance, it partly controls the behavior of volcanic eruptions. Liquidus phase relations and volume properties of magmas are also influenced by dissolved water (e.g., Kushiro, 1972; Ochs III and Lange, 1999).

Since the work of Wasserburg (1957), it is commonly assumed that water dissolved in silicate melts breaks their Si-O-Si linkages, as described by:

$$H_2O_{mol\ (melt)} + \text{Si-O-Si}_{\ (melt)} \Leftrightarrow 2\ \text{Si-OH}_{\ (melt)}\ . \qquad (1)$$

In this suggested solution mechanism, $H_2O_{mol}$ is molecular water dissolved in the melt. The Si-OH bonds are formed through $H_2O_{mol}$ dissociation into $OH^-$ groups via reaction with Si-O-Si bonds. A consequence of reaction (1) is depolymerization of the silicate melt structure, which, in turn, may lead to changes in its physical properties. For example, this simple

solution mechanism explains qualitatively the decrease of the viscosity of aluminosilicate melts observed upon water addition (Richet et al., 1996).

Infrared absorption studies of hydrous glasses and melts have demonstrated the presence of both $OH^-$ groups and $H_2O_{mol}$ species (Davis and Tomozawa, 1996; Efimov and Pogareva, 2006; Malfait, 2009; Scholtze, 1960; Stolper, 1982). Results of recent NMR spectroscopic studies of depolymerized silicate glasses (Cody et al., 2005; Mysen and Cody, 2005; Xue and Kanzaki, 2004, 2006, 2007, 2008) have led to the suggestion that water also can react with alkali and alkaline earth, *M*, network modifying cations to form M-OH bonds in depolymerized melts. Results from thermodynamic modeling of silicate melts (Moretti, 2005; Moretti et al., 2014) and Raman studies (Le Losq et al., 2013; Mysen and Virgo, 1986a,b) reinforce such hypothesis. Notably, whereas formation of T-OH bonds (T=tetrahedrally coordination cations such as $Si^{4+}$ and $Al^{3+}$) in melts might cause network depolymerisation, formation of M-OH bonds may lead to melt polymerization (e.g., Fraser, 1977; Moretti, 2005; Moretti et al., 2014; Xue and Kanzaki, 2004, 2006, 2007, 2008).

Temperature controls the ratio of $OH^-$ to $H_2O_{mol}$ species in silicate melts (Behrens and Yamashita, 2008; Nowak and Behrens, 1995; Shen and Keppler, 1995). The effect of the melt chemistry is less evident. Most studies focus on glasses, which preserve a record of the structure of melts at their glass transition temperature (*Tg*). The latter depends on water content and on silicate composition (see for a review Mysen and Richet, 2005). It follows that the $OH^-/H_2O_{mol}$ ratio in glasses is not only affected by the chemical composition of the precursor melts, but also by their *Tg* because of the temperature control over the water speciation (Ohlhorst et al., 2001). Therefore, chemical effects on water speciation in melts cannot be accomplished when the glasses have different glass transition temperatures. We note, however, that the *in situ* FTIR study at high temperature of Behrens and Yamashita

(2008) suggested that chemical effects on the water speciation could be quite important. Indeed, the equilibrium constant of the $H_2O_{mol}$ dissociation into $OH^-$ species ($H_2O + O^{2-} = 2OH^-$) in simple sodium silicate melts is quite different from those previously determined *in-situ* for rhyolitic aluminosilicate compositions (Nowak and Behrens, 1995; Shen and Keppler, 1995; Sowerby and Keppler, 1999). However, Behrens and Yamashita (2008) emphasized that the existing dataset is too small to provide sufficient information to infer water speciation and its environment in most silicate melts, and, hence, in natural magmas.

In order to provide better insights into the chemical effects on the $OH^-/H_2O_{mol}$ behavior and the proton environment in amorphous silicate materials, we choose to study simple alkali tetrasilicate glasses ($K_2Si_4O_9$, $Na_2Si_4O_9$, $Li_2Si_4O_9$). By varying the type of the alkali metal in the glasses, their effect on the water speciation can be evaluated. The chosen glasses present a significant advantage in their relatively similar glass transition temperatures (difference in the 30 K range) and viscosities (see Bockris et al., 1955; Poole, 1949). Therefore, observations made on the glasses will reflect mainly chemical effects rather than a temperature effect, thus minimizing the difficulties previously discussed. To study the proton environment in the glasses, $^1$H MAS NMR spectroscopy was used. This technique brings information about the environment of protons as well as the speciation of water in hydrous glasses (see for instance the studies of Eckert et al., 1988; Kohn et al., 1989; Robert et al., 2001; Schaller and Sebald, 1995).

## Experimental methods

### *Sample preparation and water determination*

Starting compositions were anhydrous KS4 ($K_2Si_4O_9$), NS4 ($Na_2Si_4O_9$) and LS4

($Li_2Si_4O_9$) glasses, composed of 20 mol% $M_2O$ (with M = Li, Na, K) and 80 mol% $SiO_2$ (Table 1). The glasses were synthesized by mixing pure anhydrous $SiO_2$, $K_2CO_3$, $Na_2CO_3$ and $Li_2CO_3$ powders followed by grinding under ethanol for about 1 hour. The oxide + carbonate mixtures were first decarbonated by placing the samples in a high-temperature, ambient-pressure furnace in a Pt crucible. In this step, temperature was increased by about 1.5°/min until reaching 1000°C. This decarbonation step was followed by a further temperature increase for melting near 1200°C for the KS4 glass, 1400 °C for the NS4 glass, and 1630°C for the LS4 glass. These final temperatures were governed by the respective liquidus temperatures of the materials (Eppler, 1963; Schairer and Bowen, 1955, 1956). Melts were quenched to glass by placing the bottom of the crucible in liquid $H_2O$. The resulting glasses were crushed to a powder under ethanol before the preparation of platinum capsules for high-pressure, high-temperature experiments. These crushed powders were heated at 400°C for 1 hour to ensure complete removal of ethanol and stored at 110°C before loading in capsules for high-temperature/-pressure experiments to avoid reaction with atmospheric water before an experiment. Such effect is particularly critical for the KS4 glass (Schairer and Bowen, 1955). The NS4 and KS4 starting glasses are transparent, and chemically homogeneous (Table 1). Both observations indicate that NS4 and KS4 glasses are not phase-separated (in accordance with the phase relations of these compositions; Kracek, 1932; Schairer and Bowen, 1955, 1956). Phase separation and crystallization may be issues for making the LS4 glass, because of the presence of a miscibility gap near 1000°C and of a tendency to crystalize lithium disilicate (Eppler, 1963; Haller et al., 1974; Kracek, 1930). However, by heating this melt at high temperature (>1600 °C) and quenching it at a rate ≥ 500°C/s, we obtained a transparent glass, without "milky" appearance typical of phase-separated glasses. Furthermore, analysis of the glass showed it to be chemically homogeneous chemistry.

To prepare hydrous glasses from melts at high temperature and pressure, the starting materials were contained in ~10 mm long, 5 mm diameter platinum capsules. The appropriate amount of water was added first (from ~1 to ~12 µl) with a microsyringe (precision ±0.1 µl). The exact amount of water was determined by weighing the capsule after addition of water. The crushed, anhydrous silicate glass was then added (typically 150 to 180 x $10^{-5}$ g) and the capsules were welded shut. A final weighing step was performed to check if capsules were perfectly sealed by weighing them before and after heating to 300°C for 1 hour. The samples were then placed in ¾"-diameter furnace assemblies based on the design of Kushiro (1976) and subjected to the desired pressure (1.5 GPa) and temperature (1450˚-1650˚C) for 90 minutes in a solid-medium, high-pressure apparatus (Boyd and England, 1960) (see Table 2). Temperatures were measured with type S thermocouples with no correction for pressure on their *emf*, which may be as much as 10°C (Mao et al., 1971). Pressure was calibrated against the melting point of NaCl and the calcite-aragonite transformation (Bohlen, 1984). Estimated uncertainties are ~10°C and ~0.1 GPa, respectively.

To determine water concentrations of glasses, several analytical approaches were used. First, the NS4 glasses were analyzed by FTIR spectroscopy with a Jasco® IMV-4000 infrared multi-channel infrared spectrometer and using the protocol of Yamashita et al. (2008). Samples were initially double-polished using oil at a thickness of around 100 µm. Transmission spectra were recorded with a 10X objective and a 100 × 100 µm aperture. A 6-order polynomial baseline was employed for subtracting the background in the frequency range of interest (4000 - 5800 $cm^{-1}$) The extinction coefficients provided in Yamashita et al. (2008, see their table 4, protocol A) were used to retrieve the concentrations of $OH^-$ and $H_2O_{mol}$ species from the integrated areas beneath the ~4500 and ~5200 $cm^{-1}$ absorption bands. The water concentration of the LS4 and KS4 glasses was determined with Raman

spectroscopy because molar absorption coefficients are not available for these glass compositions. The Raman spectrometer was a Jasco® NRS 3100 spectrometer equipped with a notch filter, holographic gratings, a single monochromator, and a 1024x128 Andor® DV401-F1 CCD Peltier-cooled at -69°C. Spectra were collected between 350 and 4000 $cm^{-1}$ with 1200 lines/mm grating. The samples were excited with a 490 nm solid state Coherent™ laser, focused ~10 µm below the glass surface through a 50x Olympus® lens. Laser power at the sample was 44 mW. To determine the water concentration of the glasses, a calibration relating the area of the Raman band attributed to the OH stretching signal to the FTIR-based NS4 glass water concentration was implemented, using a protocol similar to that of Le Losq et al. (2012) (see details in Appendix 1). The area of the Raman OH stretching signal was normalized to that of the Raman silicate signals (located below 1500 $cm^{-1}$), so that, this calibration does not depend on glass chemistry (Le Losq et al., 2012; Shea et al., 2014). Raman-derived water concentrations for LS4 agree with Loss on Ignition (see the protocol described in the next paragraph and Table 2), reinforcing the previous statement. The water concentrations of glasses are shown in Table 2.

A final check of water concentrations was carried out by measuring Loss On Ignition (LOI) by using the fine (< 5 microns) powders also employed for NMR experiments. These powders were first dried one night at 180 °C. Then, weigh loss was measured between 180 °C and 1100 °C. Consistent and reproducible results were obtained for the LS4 glasses (Table 2), but not for the NS4 and KS4 glasses. For those glasses, erratic LOI at 180°C, ranging from 1.5 up to 5.0 wt%, indicate that the powders adsorbed atmospheric water. LOI were performed several weeks after the NMR measurements (the powders were obtained right before, see below). Despite the precautions adopted to minimize the time they spent in atmosphere, water adsorption by the NS4 and KS4 powders in such a long timescale is not

surprising regarding their low granulometry (Newman et al., 1986) and the very hygroscopic nature of NS4 and KS4 glasses (Schairer and Bowen, 1955, 1956).

Because of the pronounced hygroscopic nature of the alkali silicate glasses, particularly of the KS4 composition, the maximum time the starting materials were exposed to ambient atmospheric conditions was minimized. Raman and FTIR spectra of hydrous glasses were acquired, therefore, immediately after their synthesis. In addition, Raman spectra were acquired by focusing the laser beam inside the sample (not at the surface). Moreover, the FTIR spectra analyze a large bulk part of samples. Such analysis conditions ensure that the water IR and Raman signals arise from "structural" water, i.e. water dissolved in the structure of the melt at high pressure and temperature prior to quenching to a hydrous glass. The glass chips from the high-pressure experiments were crushed to powder immediately before performing the NMR experiments. Even so, during the loading of rotors and the installation of the probe, the powder remained in contact with the atmosphere for 30-60 minutes. During the experiments, the powdered sample was spinning at 22 kHz in dry air. This ensures optimal conditions for analyzing powders without hydration. As a result, the $^{1}$H NMR signal is representative of water quenched in the glass from the melt.

*Solid-state Nuclear Magnetic Resonance (NMR) spectroscopy*

Hydrogen-1 solid-state NMR experiments were carried out with a Chemagnetics CMX Infinity 300 Solid State NMR. The static field strength of the magnet is ~7.05 T. The Larmor frequency of $^{1}$H is ~300 MHz. Samples were loaded in 2.5mm diameter zirconia rotors, which were placed in a Chemagnetic double resonance probe. Average sample mass was ~12 mg. In order to ensure that only the $^{1}$H signal from the sample was detected (i.e., not from outside the RF coil), a 16-cycle DEPTH sequence was used. This pulse sequence employs four 90 °

193 pulses at select phases and a cycle of 16 pulses to cause $^{1}H$ with a nutation of less than $\pi/4$
194 (e.g., outside the RF coil) to lose coherence. Only $^{1}H$ nucleii inside the coil can experience a
195 nutation angle of $\pi/2$ and will retain coherence and contribute to the acquired signal. The $^{1}H$
196 pulse length was 2.5 μs, with a 100 s recycle delay and 1600 acquisitions. The Magic Angle
197 Spinning (MAS) frequency ($\omega_r/2\pi$) was 22 kHz. All spectra were referenced to
198 tetramethylsilane.
199 In order to determine the number of components needed to account for the variance of
200 data, the principal component analysis (PCA) algorithm of the Scikit-learn Python package
201 was used (Pedregosa et al., 2011).
202
203 **Results**
204 The $^{1}H$ MAS NMR spectra of hydrous LS4 glasses comprise an asymmetric resonance
205 peak centered at 3.7 ppm. The asymmetry reflects a shoulder near 15 ppm and a small peak at
206 1.3 ppm (Figure 1, top). The intensity of the main 3.7 ppm peak increases strongly with
207 increasing water concentration. The 1.3 ppm contribution is sharp and intense in the spectrum
208 of LS4 + 3.3 mol% $H_2O$, and becomes weaker relative to the main 3.7 ppm peak in the
209 spectrum of LS4 + 9.4 mol% $H_2O$. With 17.6 mol% $H_2O$ in the LS4 glass, only a small
210 shoulder on the right side of the 3.7 ppm main peak is observed. The intensity of the shoulder
211 at ~15 ppm also increases with increasing water concentration.
212 The intensity patterns of the $^{1}H$ MAS NMR spectra of the NS4 hydrous glasses differ
213 significantly from those of hydrous LS4 glasses (Figure 1, middle). The main contribution to
214 the spectra of hydrous NS4 glass is located at 15.9 ppm. This peak is asymmetric, suggesting
215 the presence of another contribution near ~13 ppm. Two other peaks are visible at 4.0 and 1.1
216 ppm, the latter being the sharpest and most symmetric among the peaks in the $^{1}H$ MAS NMR

spectra of hydrous NS4 glasses. The 15.9 and 4.0 ppm peaks intensities increase with increasing water content, whereas the 1.1 ppm peak intensity remains constant. This latter behavior is similar to that observed in $^{1}$H MAS NMR spectra of the hydrous LS4 glasses. The ~4 ppm maximum splits in two shoulders at 3.5 ppm and 4.6 ppm at 17.6 mol% $H_2O$ (Figure 1, middle).

In the case of the hydrous KS4 glasses, most of the $^{1}$H MAS signal is near 16.0 ppm in the form of an asymmetric peak somewhat similar to the 16 ppm peak in the spectra of hydrous NS4 glasses (Figure 1, bottom). However, the intensity at frequencies lower than ~10 ppm is considerably less pronounced in the spectra of hydrous KS4 compared with those of hydrous NS4 (Figure 1, middle and bottom). At all water contents, there is also a small peak at 1.2 ppm. At 9.4 mol% $H_2O$, there is an intensity increase of the 16.0 ppm peak, whereas that of the 1.2 ppm peak remains constant, and a small shoulder near ~5 ppm appears. A further increase of water concentration to 17.6 mol% $H_2O$ results in increased intensity of the 16.0 ppm peak and ~5 ppm shoulder, which forms a small broad peak at this water content.

In the spectra of hydrous LS4 and NS4 glasses, the intensity of sidebands increases with increasing water concentration (Figure 2). At the same water content, sideband intensities are significantly higher in NMR spectra of hydrous LS4 glasses compared with those of hydrous NS4 glasses. There is little or no sideband intensity in the $^{1}$H MAS NMR spectra of hydrous KS4 glass at any water content.

To identify more clearly the spectral changes as a function of the ionic radius of the alkali metal and of water addition, the portions of signal in the three main visible bands located at ~16.0 ppm, ~4.5 ppm and ~1.3 ppm will be considered. To do so, the spectra were divided in three frequency ranges, the "low frequency" (LF) portion between -30 and 1.8 ppm, the "middle frequency" (MF) one between 1.81 and 7.7 ppm, and the "high frequency" (HF)

241 portion from 7.7 up to 30 ppm (HF). When the ionic radius of the alkali increases, the $H^+$
242 contributions in the HF domain increase of ~200% (Figure 3). In parallel, the $H^+$ contributions
243 to the MF domain strongly decrease. The area of the LF domain tends to decrease with
244 increasing the ionic radius of alkali. The water concentration has a much smaller effect (in the
245 1 – 10% range) than the ionic radius of alkali on the fraction of $H^+$ giving signals in the LF,
246 MF and HF domain (Figure 3).
247
248 **Discussion**
249 Observations summarized in figures 1-3 indicate that the ionic radius of alkalis
250 strongly affect the $^1$H MAS NMR signal, whereas total water concentration has a smaller
251 effect. The presence of peaks near 1.0, 5.0 and 16.0 ppm, and of shoulders near 3.5 and 12.0
252 ppm, indicate that four and perhaps five spectral components, centered at the corresponding
253 frequency, may be necessary to describe the entire $^1$H MAS NMR spectra of the glasses
254 (Figure 1). Analysis of the dataset with principal component analysis PCA shows that 4
255 components account for 99.64% of the variance of the data, and 5 for 99.85 (Table 3).
256 Therefore, the visual observation and statistical treatment of $^1$H NMR spectra indicate the
257 presence of at least five components near 1.0, 3.5, 5.0, 12.0 and 16.0 ppm. The type of alkali
258 metal in the glass affects the relative intensities of those components but not their frequencies
259 (Figure 1). Therefore, the effect of changing the ionic radius of the alkali metal in the silicate
260 glasses is to change the distribution of $H^+$ among five structural environments.
261
262 *Origin of the $^1$H NMR signals*
263 Sideband analysis aids in the structural interpretation of the NMR spectra. To obtain a
264 quantitative isotropic $^1$H NMR signal, the $^1$H-$^1$H dipolar coupling was averaged out by using

magic angle spinning. Any residual dipolar coupling will be manifested by spinning side bands at $\pm n\omega_r/2\pi$ (n=1, 2, …). For instance, for $H_2O_{mol}$ entities in a rigid environment (e.g., immobile $H_2O$ molecules), the $^1H$-$^1H$ dipolar coupling is on the order of 36 KHz. Therefore, as we spin at 22 kHz, a signal from rigid $H_2O_{mol}$ entities would be expected. However, molecular $H_2O_{mol}$ at room temperature in glasses have slight motions (see Eckert and Yesinowski, 1987) that will reduce the intensity of sidebands, because such motions contribute to average out the $^1H$-$^1H$ dipolar coupling. Isolated $OH^-$ groups will not contribute to sideband intensity. In a rigid environment, the sideband signal from $OH^-$ groups is governed by the $^1H$ chemical shift anisotropy together with homonuclear and heteronuclear interactions. It is negligible compared to the sideband signal from $H_2O_{mol}$ species (Eckert et al., 1988). Consequently, the intensity of sidebands in the $^1H$ MAS NMR spectra of hydrous alkali silicate glasses mostly reflects the presence and concentration of $H_2O_{mol}$ species (Figure 2).

Cody et al. (2005) demonstrated that the sidebands in $^1H$ MAS NMR spectra of hydrous $SiO_2$ and NS4 glasses primarily are correlated with a central peak near 6.4 ppm, which would suggest $H_2O_{mol}$. Kohn et al. (1989) also attributed a peak near 5 ppm in $^1H$ MAS NMR spectra of silica and silicate glasses to $H_2O_{mol}$ species. Additional support for such an assignment is provided in the 2D $\{^1H\}$-$^{29}Si$ HETCOR experiment on hydrous NS4 glasses of Robert et al. (2001), who noticed missing intensity near 4 ppm compared to 1D $^1H$ MAS NMR experiments. This means that some protons are not cross-polarized with silicon and, thus, would be in molecules of water (Robert et al., 2001). In the spectra of the NS4 glasses (Figure 1), the shoulder near 5 ppm appears with increasing the water concentration. This development is accompanied by increasing sideband intensities (Figure 2). As a result, and in agreement with the studies of Cody et al. (2005), Kohn et al. (1989), the 5 ppm contribution

289 in the spectra reported here likely is a record of signals of $H^+$ in $H_2O_{mol}$ species. According to
290 Cody et al. (2005), Kohn et al. (1989), Robert et al. (2001) and Xue and Kanzaki (2004), the
291 3.5 ppm contribution might arise mainly from signal of $H^+$ in Si-OH bonds, forming weak
292 hydrogen bonds with their environments.

293 The sideband intensities in the $^1$H MAS NMR spectra of hydrous KS4 glasses are
294 negligible, whereas the 12 and 16 ppm contributions are particularly strong (Figures 1, 2).
295 Therefore, these two contributions likely reflect $H^+$ in $OH^-$ groups bonded to cationic entities
296 in the glass structure. The $\{^1H\}$-$^{29}$Si HETCOR experiments of Robert et al. (2001) performed
297 on an NS4 hydrous glass (1.28 wt% $H_2O$) are consistent with the 16, 12 and 3.5 ppm $^1$H NMR
298 lines all correlated with $^{29}$Si NMR signals of $Q^3$ and $Q^2$ tetrahedral species. Formation of $Q^2$
299 and $Q^3$ species in sodium silicate glasses is observed upon hydration (Cody et al., 2005;
300 Mysen and Cody, 2005; Zotov and Keppler, 1998). According to those observations, the 12
301 and 16 ppm contributions record signals from $OH^-$ bonded to Si, forming the so-called Si-OH
302 groups. However, Cody et al. (2005) also found that the intensity of the 12 ppm peak
303 increases with increasing Na/Si ratio of the glass, which might not be consistent with an
304 assignment of this peak to only Si-OH groups. Furthermore, for the sodium disilicate glass
305 (Na/Si = 1), the $H_2O_{mol}/OH^-$ ratio predicted by using the distribution of $Q^n$ species distribution
306 was too high compared with that inferred from the $^1$H NMR spectrum. Combining this
307 observation with considerations about the relaxation times of $Q^n$ species, Cody et al. (2005)
308 concluded that at high Na/Si, some Na-OH groups must exist and may result in a signal close
309 to 12 ppm. Therefore, we cannot rule out that some of the signal that contribute to the 12 ppm
310 peak in KS4, NS4, and LS4 hydrous glasses may reflect alkali-OH bonding. This assignment
311 does not disagree with the HETCOR experiment of Robert et al. (2001), because those
312 experiments probe the proximity of $Q^n$ species to protons and not their link. However, the

313 correlation implies that M-OH groups interact with $Q^n$ species, through hydrogen bonding for
314 example.

315 The $^1$H NMR signal near 1.0-1.7 ppm may arise from "free" M-OH groups, i.e. which
316 do not form hydrogen bonds with their environment, according to the work of Xue (2009),
317 Xue and Kanzaki (2004), and Xue and Kanzaki (2009). However, the assignment of the peak
318 near 1 ppm is not totally clear. For example, Si-OH groups without hydrogen bonding can
319 give signals near 1 - 2 ppm, as shown by proton NMR of silica gels (see Bronnimann et al.,
320 1988 for instance). Xue and Kanzaki (2004) ruled out such an Si-OH attribution because of
321 the absence of a clear peak near 1 ppm in the Suprasil silica glass, which contains low water
322 concentration (~1200 ppm, and therefore mostly dissolved as $OH^-$ group, see the $^1$H MAS
323 NMR spectra in Kohn et al., 1989). However, without more information, the precise
324 assignment of the ~1 ppm peak remains uncertain. But whatever the X cation (X = Si or M)
325 involved in the X-OH bond giving rise to this peak may be, existing data indicate that the $OH^-$
326 do not form hydrogen bonds with their environment.
327
328 *$O^{\cdots}O$ distances of the various $H^+$ environments*

329 The $^1$H NMR chemical shift in hydrous oxide systems is predominantly dependent on
330 the O-H distance, and thus on the O-O distance along the O-H$^{\cdots}$O bond (with $^{\cdots}$ an hydrogen
331 bond; Berglund and Vaughan, 1980; Eckert et al., 1988; Xue and Kanzaki, 2001, 2009).
332 Indeed, hydrogen bonding pulls the $^1H^+$ away from the bonding oxygen, which results in
333 deshielding of the $^1$H and in an increase of its resonant frequency. It follows that the NMR
334 peaks near 1.0, 3.5, 5.0, 12.0 and 16.0 ppm reflect five environments in the glasses with
335 different mean O-O distances. These distances can be estimated with an uncertainty near ± 10
336 pm by using the equation from Eckert et al. (1988) (Figure 4).

337 The 3.5 ppm Si-OH signal is related to an environment with an O-O mean distance of
338 ~295 pm, a value similar to that the ~290 pm O-O distance of the $H_2O_{mol}$ species
339 environment. According to the models of Xue and Kanzaki (2004), Si-OH groups in different
340 tetrahedral units and connected between them through hydrogen bonding (Si-OH···O(H)Si
341 entities) are good candidates for the 295 pm Si-OH environment. The correlation between the
342 $^1$H signal near 3 ppm and that of $Q^4$ units in the HETCOR data of Robert et al. (2001) also
343 indicates that the occurrence of Si-OH···BO bonds is plausible (with BO a bridging oxygen
344 connecting two $SiO_4$ tetrahedra). Finally, the formation of Si-OH···$OH_2$ ($OH_2$ being a water
345 molecule) cannot be excluded. Figure 4 summarizes all the proposed attributions.

346 The $OH^-$ groups in the 261 and 250 pm environments reflect O-O distances that are
347 shorter or nearly equal to that of the typical anhydrous O-O distances in LS4/NS4 glasses
348 (262 pm, Ispas et al., 2010). Those two environments can record signals from:

349 (i) Si-OH groups forming "intratetrahedral" hydrogen bonds. Kohn et al. (1989)
350 proposed this hypothesis to account for the presence of the $^1$H NMR signal
351 between 11 and 17 ppm in hydrous silicate glasses. As the distance between
352 O species on a same tetrahedral edge in a single tetrahedron is close to 264
353 pm, the 261 pm environment may be a good candidate for this attribution.
354 Such "intratetrahedral" hydrogen bonds are observed in crystalline hydrous
355 sodium disilicate (Ai et al., 2002, 2003)

356 (ii) Si-OH groups connected to other tetrahedral units through strong hydrogen
357 bonds with NBO species (Si-OH···O(M)Si bonds), because of the increasing
358 hydrogen bonding strength accompanying introduction of nonbridging
359 oxygen in glasses (Xue and Kanzaki, 2004).

360 (iii) Si-O[H]-M groups, where the Si-O-M bonds are protonated. Here the protons

assist in the electronic balance of NBO when the O-M distance is high (in the case of K-bearing silicate glasses for instance).

(iv) M-OH groups, as suggested by Cody et al. (2005) for the 261 pm environment. Those M-OH groups must form short hydrogen bonds with surrounding oxygens (M-OH···NBO/BO linkages).

It is difficult to discriminate between those hypotheses, and a combination of all of them is possible. For instance, the formation of M-OH···NBO/BO bonds, which could result in a signal near 12 ppm as suggested by the data of Cody et al. (2005), may lead to the $Q^n$-H interactions observed in the HETCOR spectra of Robert et al. (2001). At the same time, the $Q^n$ distribution in hydrous NS4 glasses also indicates that $OH^-$ groups are mostly involved in Si-OH bonds in those glasses (see also Cody et al., 2005; Mysen and Cody, 2005; Zotov and Keppler, 1998). In addition to that, the $^{23}$Na 1D MAS NMR and $\{^1H\}$-$^{23}$Na REDOR NMR experiments of Robert et al. (2001) indicate that the environment of Na in NS4 hydrous glasses does not seem to vary with water content. This interpretation does not support the presence of significant amount of Si-O[H]-M protonated bonds, or of M-OH bonds. Therefore, in the compositions examined in the present study, the high-frequency 12 and 16 ppm $^1$H signals may arise mostly from Si-OH bonds, with the $H^+$ forming strong inter- or intra-tetrahedral hydrogen bonds with the surrounding oxygen atoms.

*Origin of the chemical effects on the $H^+$ environments*

From the data and discussion above (Figures 1, 2, 3, 4), decreasing ionic field strength of the alkali cation, which acts as network modifiers in silicate glasses, promotes the dissociation of $H_2O_{mol}$ into $H^+$ and $OH^-$. Those ionic entities react with the Si-O-Si and Si-O-M bonds to form Si-OH bonds, with the $H^+$ forming stronger hydrogen bonds the greater the

ionic radius of alkali. The formation of M-OH bonds cannot be ruled out and could contribute to the $^{1}$H NMR signals near 12 or 1 ppm, but, according to available data, probably is of minor importance at the silica concentration we studied. In any case, $^{1}$H MAS NMR data indicate that the ionic radius of alkalis, and hence their ionic field strength, controls the dissociation constant of $H_2O_{mol}$ species as well as the proton environment. The origin of such control can arise from different effects, but present data do not shed light on it. We can only propose hypothesis about it. For instance, it may arise from electronic/steric effects around alkali and along the M-O-Si bonds that control the $H_2O_{mol}$ dissociation constant as well as the strength of hydrogen bonding. It may also arise from the tendency to form $H_2O_{mol}$ hydration shells around small alkalis (explaining the high $H_2O_{mol}$ concentration in LS4 compositions for instance; such effect is observed in hydrous solutions, see for instance Mähler and Persson, 2012). Simple volume effects can also be proposed: the higher the alkali radius, the lower the volume available for protons, this promoting $H_2O_{mol}$ dissociation in $OH^-$ groups that can occupy environments with smaller O-O distances.

## Implications

The influence of the alkali radius on the mean O-O distance around protons (Figure 4) implies significant modification of the mean volume of water molecules. Assuming that the O-O distances around protons in glasses represent the diameters of the oxygen coordination sphere of protons, the mean volume of this sphere can be calculated using the sum of the O-O distances pondered by their associated relative $^{1}$H NMR intensity (hence proton population). For a given glass composition, this mean volume does not vary significantly with water concentrations, because the water concentration does not change the $^{1}$H NMR signal significantly (Figure 3). In contrast to that conclusion, increasing the ionic radius of alkali

produces a decrease of the mean volume of the proton coordination sphere (Figure 5). There is, for example, a 15.8 % volume difference between the NS4 and KS4 glasses. The partial molar volumes of $H_2O$ in the NS4 and KS4 melts, determined by Mysen and Cody (2004) by using solubility measurements and the Gibbs-free energy of solution of $H_2O$ (Figure 5), differ by 16.9 %. Considering the errors affecting the determinations of the partial molar volume of $H_2O$ and those of the mean volumes of the protons coordination sphere calculated from $^1H$ NMR spectra, those variations are in very good agreement. Therefore, it is suggested that the change of the distribution of $H^+$ in various structural environments explains the observed decrease of the partial molar volume of $H_2O$ that occurs upon increasing the ionic radius of alkalis in silicate melts. As a consequence, it appears that the effects of the ionic radius of alkalis on the water speciation and on the proton environment may govern the variation of the partial molar volume of $H_2O$ in silicate melts. Such relationships will impact the buoyancy of magmas, and also the solubility of water. Indeed, the water solubility is systematically higher in NS4 melts than in KS4 melts (Mysen, 1998; Mysen and Cody, 2004). This leads to the suggestion that, if larger structural sites are available for storing $H_2O_{mol}$ and $OH^-$ species, the water solubility will be higher.

In summary, this study demonstrates that the chemical composition of silicate melts and glasses can play an important role in defining the speciation of water and the proton environment. This results in variations in the solubility and partial molar volume of water in magmas. Such a complex relationship will play a critical role in determining the degassing path and the density of a rising magma, and hence will affect in various ways the behavior of volcanic eruptions.

**Acknowledgments**

We thank John Armstrong (GL-CIW) for his help with S.E.M analysis of glasses and Roxane Bowden (GL-CIW) for her help for measurements of $H_2O$ concentrations. We also thank two anonymous reviewers and the associate editor Don Baker for their comments that helped improve the manuscript. This research was partially supported by grant EAR1212754, to B.O.M. and the NASA Astrobiology Institute. All NMR experiments were performed at the W. M. Keck Solid State NMR Facility at the Geophysical Laboratory, supported in part by the W. M. Keck Foundation and the Carnegie Institution of Washington.

## References

Ai, X., Chen, L., Dong, J., Ye, C., and Deng, F. (2003) Variation of sodium coordination during the hydration processes of layered sodium disilicates as studied by $^{23}$Na MQMAS and $^{1}$H <-> $^{23}$Na CP/MAS NMR spectroscopy. Journal of Materials Chemistry, 13, 614-621.

Ai, X., Deng, F., Dong, J., Chen, L., and Ye, C. (2002) Stability of layered sodium disilicate during hydration process as studied by multinuclear solid state NMR spectroscopy. Journal of Physical Chemistry B, 106, 9237-9244.

Behrens, H., and Yamashita, S. (2008) Water speciation in hydrous sodium tetrasilicate and hexasilicate melts: Constraint from high temperature NIR spectroscopy. Chemical Geology, 256, 306-315.

Berglund, B., and Vaughan, R. W. (1980) Correlations between proton chemical shift tensors, deuterium quadrupole couplings, and bond distances for hydrogen bonds in solids. The Journal of Chemical Physics, 73, 2037-2043.

Bockris, J. O., MacKenzie, J. D., and Kitchener, J. A. (1955) Viscous flow in silica and binary liquid silicates. Transactions of the Faraday Society 51, 1734-1748.

Bohlen, S. R. (1984) Equilibria for precise pressure calibration and a frictionless furnace assembly for the piston-cylinder apparatus. Neues Jahrbuch für Mineralogie Mh., 84, 404-412.

Boyd, F. R., and England, J. L. (1960) Apparatus for phase-equilibrium measurements at pressures up to 50 Kilobars and temperatures up to 1750 °C. Journal of Geophysical Research, 65, 741-748.

Bronnimann, C. E., Zeigler, R. C., and Maciel, G. E. (1988) Proton NMR study of dehydration of the silica gel surface. Journal of the American Chemical Society, 110, 2023-2026.

Cody, G. D., Mysen, B. O., and Lee, S. K. (2005) Structure vs. composition: A solid-state $^{1}$H and $^{29}$Si NMR study of quenched glasses along the $Na_2O$-$SiO_2$-$H_2O$ join. Geochimica et Cosmochimica Acta, 69, 2373-2384.

Davis, K. M., and Tomozawa, M. (1996) An infrared spectroscopic study of water-related species in silica glasses. Journal of Non-Crystalline Solids, 201, 177-198.

Eckert, H., and Yesinowski, J. P. (1987) The state of water in rhyolitic glasses, A deuterium

472 NMR study. Journal of Non-Crystalline Solids, 93, 93-114.
473 Eckert, H., Yesinowski, J. P., Silver, L. A., and Stolper, E. M. (1988) Water in silicate
474 glasses: quantification and structural studies by $^{1}H$ solid echo and MAS-NMR methods.
475 Journal of Physical Chemistry, 92, 2055-2064.
476 Efimov, A. M., and Pogareva, V. G. (2006) IR absorption spectra of vitreous silica and
477 silicate glasses: the nature of bands in the 1300 to 5000 $cm^{-1}$ region. Chemical Geology,
478 229, 198-217.
479 Eppler, R. A. (1963) Glass formation and recrystallization in the lithium metasilicate region
480 of the system $Li_2O$-$Al_2O_3$-$SiO_2$. Journal of the American Ceramic Society, 46, 97-101.
481 Fraser, D. G. (1977) Thermodynamic properties of silicate melts. in Thermodynamics in
482 Geology, pages 301-325, D. Reidel Publishing Company.
483 Haller, W., Blackburn, D. H., and Simmons, J. H. (1974) Miscibility gaps in alkali-silicate
484 binaries - Data and thermodynamic interpretation. Journal of the American Ceramic
485 Society, 57, 120-126.
486 Ispas, S., Charpentier, T., Mauri, F., and Neuville, D. R. (2010) Structural properties of
487 lithium and sodium tetrasilicate glasses: Molecular dynamics simulations versus NMR
488 experimental and first-principles data. Solid State Sciences 12, 183-192.
489 Kohn, S. C., Dupree, R., and Smith, M. E. (1989) Proton environments and hydrogen-bonding
490 in hydrous silicate glasses from proton NMR. Nature, 337, 539-541.
491 Kracek, F. C. (1932) The ternary system: $K_2SiO_3$-$Na_2SiO_3$-$SiO_2$. The Journal of Physical
492 Chemistry, 36, 2529-2542.
493 Kracek, F. C. (1930) The binary system $Li_2O$-$SiO_2$. The Journal of Physical Chemistry 12,
494 2641-2650.
495 Kushiro, I. (1972) Effect of water on the composition of magmas formed at high pressures.
496 Journal of Petrology, 13, 311-334.
497 Kushiro, I. (1976) A new furnace assembly with a small temperature gradient in solid-media,
498 high-pressure apparatus. Carnegie Institution of Washington Year Book, 75, 832-833.
499 Le Losq, C., Moretti, R., and Neuville, D. R. (2013) On the speciation and amphoteric
500 behavior of water in aluminosilicate melts and glasses: High-Temperature Raman
501 spectroscopy and reaction equilibria. European Journal of Mineralogy, 25, 777-790.
502 Le Losq, C., Neuville, D., Moretti, R., and Roux, J. (2012) Determination of water content in
503 silicate glasses using Raman spectrometry: implications for the study of explosive
504 volcanism. American Mineralogist, 97, 779-790.
505 Le Losq, C., Neuville, D. R., Florian, P., Henderson, G. S., and Massiot, D. (2014) The role
506 of $Al^{3+}$ on rheology and structural changes of sodium silicate and aluminosilicate
507 glasses and melts.. Geochimica et Cosmochimica Acta, 126, 495-517.
508 Malfait, W. J. (2009) The 4500 $cm^{-1}$ infrared absorption band in hydrous aluminosilicate
509 glasses is a combination band of the fundamental {Si,Al}-OH and O-H vibrations.
510 American Mineralogist, 94, 849-852.
511 Mao, H. K., Bell, P. M., and England, J. L. (1971) Tensional errors and drift of the
512 thermocouple electromotive force in the single stage, piston-cylinder apparatus.
513 Carnegie Institution of Washington Year Book, 70, 281-287.
514 Moretti, R. (2005) Polymerisation, basicity, oxidation state and their role in ionic modelling
515 of silicate melts. Annals of Geophysics, 48, 583-608.
516 Moretti, R., Le Losq, C., and Neuville, D. R. (2014) The amphoteric behavior of water in
517 silicate melts from the point of view of their ionic-polymeric constitution. Chemical
518 Geology, 367, 23-33.
519 Mysen, B. O. (1998) Interaction between aqueous fluid and silicate melt in the pressure and

temperatures regime of the Earth's crust and upper mantle. Neues Jahrbuch für Mineralogie, 172, 227-244.

Mysen, B. O., and Armstrong, L. (2002) Solubility behavior of alkali aluminosilicate components in aqueous fluids and silicate melts at high pressure and temperature. Geochimica et Cosmochimica Acta, 66, 2287-2297.

Mysen, B. O., and Cody, G. (2005) Solution mechanisms of $H_2O$ in depolymerozed peralkaline melts. Geochimica et Cosmochimica Acta, 69, 5557-5566.

Mysen, B. O., and Cody, G. (2004) Solubility and solution mechanism of $H_2O$ in alkali silicate melts and glasses at high pressure and temperature. Geochimica et Cosmochimica Acta, 68, 5113-5126.

Mysen, B. O., and Richet, P. (2005) Silicate glasses and melts - Properties and structure. Developments in geochemistry 10, Elsevier B.V., Amsterdam.

Mysen, B. O., and Virgo, D. (1986a) Volatiles in silicate melts at high pressure and temperature 1. Interaction between OH groups and $Si^{4+}$, $Al^{3+}$, $Ca^{2+}$, $Na^{+}$ and $H^{+}$. Chemical Geology, 57, 303-331.

Mysen, B. O., and Virgo, D. (1986b) Volatiles in silicate melts at high pressure and temperature 2. Water in melts alon the join $NaAlO_2$-$SiO_2$ and a comparison of solubility mechanisms of water and fluorine. Chemical Geology, 57, 333-358.

Mähler, J., and Persson, I. (2012) A study of the hydration of the alkali metal ions in aqueous solution. Inorganic Chemistry, 51, 425-438.

Newman, S., Stolper, E. M., and Epstein, S. (1986) Measurement of water in rhyolitic glasses: Calibration of an infrared spectroscopic technique. American Mineralogist, 71, 1527-1541.

Nowak, M., and Behrens, H. (1995) The speciation of water in haplogranitic glasses and melts determined by in situ near-infrared spectroscopy. Geochimica et Cosmochimica Acta 59, 3445-3450.

Ochs III, F. A., and Lange, R. A. (1999) The density of hydrous magmatic liquids. Science, 383, 1314-1317.

Ohlhorst, S., Behrens, H., and Holtz, F. (2001) Compositional dependence of molar absorptivities of near-infrared OH- and H2O bands in rhyolitic to basalitic glasses. Chemical Geology, 174, 5-20.

Pedregosa, F., Varoquaux, G., Gramfort, A., Michel, V., Thirion, B., Grisel, O., Blondel, M., Prettenhofer, P., Weiss, R., Dubourg, V., Vanderplas, J., Passos, A., Cournapeau, D., Brucker, M., Perrot, M., and Duchesnay, E. (2011) Scikit-learn: machine learning in python. Journal of Machine Learning Research, 12, 2825-2830.

Poole, J. P. (1949) Low-temperature viscosity of alkali silicate glasses. Journal of the American Ceramic Society, 32, 230-233.

Richet, P., Lejeune, A.-M., Holtz, F., and Roux, J. (1996) Water and the viscosity of andesite melts. Chemical Geology, 128, 185-197.

Robert, E., Whittington, A. G., Fayon, F., Pichavant, M., and Massiot, D. (2001) Structural characterization of water-bearing silicate and aluminosilicate glasses by high-resolution solid-state NMR. Chemical Geology, 174, 291-305.

Schairer, J. F., and Bowen, N. L. (1955) The system $K_2O$-$Al_2O_3$-$SiO_2$. American Journal of Science, 253, 681-746.

Schairer, J. F., and Bowen, N. L. (1956) The system $Na_2O$-$Al_2O_3$-$SiO_2$. American Journal of Science, 254, 129-195.

Schaller, T., and Sebald, A. (1995) One- and two-dimensional $^{1}H$ magic-angle spinning experiments on hydrous silicate glasses. Solid State Nuclear Magnetic Resonance, 5,

89-102.
Scholtze, H. (1960) Zur Frage der unterscheidung zwischen $H_20$-Molekeln undOH-gruppen in gläsern und mineralen. Naturwissenschaften, 47, 226-227.
Shea, T., Hellebrand, E., Gurioli, L., and Tuffen, H. (2014) Conduit- to Localized-scale degassing during Plinian Eruptions: Insights from major element and volatile (Cl and $H_2O$) analyses within Vesuvius AD 79 pumice. Journal of Petrology, 55, 315-344.
Shen, A., and Keppler, H. (1995) Infrared spectroscopy of hydrous silicate melts to 1000 °C and 10 kbar: direct observation of $H_2O$ speciation in a diamond-anvil cell. American Mineralogist, 80, 1335-1338.
Sowerby, J. R. and Keppler, H. (1999) Water speciation in rhyolitic melt determined by in-situ infrared spectroscopy. American Mineralogist, 84, 1843-1849.
Stolper, A. (1982) Water in silicate glasses: An infrared spectroscopic study. Contributions to Mineralogy and Petrology, 81, 1-17.
Wasserburg, G. J. (1957) The effect of $H_2O$ in silicate systems. Journal of Geology 65, 15-23.
Whittaker, E. J. W. and Muntus, R. (1970) Ionic radii for use in geochemistry. Geochimica et Cosmochimica Acta, 34, 945-956.
Xue, X. (2009) Water speciation in hydrous silicate and aluminosilicate glasses: Direct evidence from $^{29}$Si- $^{1}$H and $^{27}$Al- $^{1}$H double-resonance NMR. American Mineralogist, 94, 395-398.
Xue, X., and Kanzaki, M. (2004) Dissolution mechanisms of water in depolymerized silicate melts: Constraints from $^{1}$H and $^{29}$Si NMR spectroscopy and ab initio calculations. Geochimica et Cosmochimica Acta, 68, 5027-5057.
Xue, X., and Kanzaki, M. (2006) Depolymerization effect of water in aluminosilicate glasses: Direct evidence from $^{1}$H- $^{27}$Al heteronuclear correlation NMR. American Mineralogist, 91, 1922-1926.
Xue, X., and Kanzaki, M. (2007) Al coordination and water speciation in hydrous aluminosilicate glasses: Direct evidence from high-resolution heteronuclear $^{1}$H-$^{27}$Al correlation NMR. Solid State Nuclear Magnetic Resonance, 31, 10-27.
Xue, X., and Kanzaki, M. (2008) Structure of hydrous aluminosilicate glasses along the diopside--anorthite join: A comprehensive one- and two-dimensional $^{1}$H and $^{27}$Al NMR study. Geochimica et Cosmochimica Acta, 72, 2331-2348.
Xue, X., and Kanzaki, M. (2009) Proton distributions and hydrogen bonding in crystalline and glassy hydrous silicates and related inorganic materials: insights from high-resolution solid-state Nuclear Magnetic Resonance spectroscopy. Journal of the American Ceramic Society, 92, 2803-2830.
Xue, X., and Kanzaki, M. (2001) Ab initio calculation of the $^{17}$O and $^{1}$H NMR parameters for various OH groups: Implications to the speciation and dynamics of dissolved water in silicate glasses. Journal of Physical Chemistry B, 105, 3422-3434.
Yamashita, S., Behrens, H., Schmidt, B. C., and Dupree, R. (2008) Water speciation in sodium silicate glasses based on NIR and NMR spectroscopy. Chemical Geology, 256, 231-241.
Zotov, N., and Keppler, H. (1998) The influence of water on the structure of hydrous sodium tetrasilicate glasses. American Mineralogist, 83, 823-834.

## ***Appendix 1 – Water analysis with Raman spectroscopy***

In order to determine the water concentration of glasses and to avoid analyzing powders, which quickly adsorb water from ambient atmosphere, we treated the Raman spectra of glasses with a protocol similar to that described in Le Losq et al. (2012). Slight modifications were made to account for the slightly different OH stretching signal in Raman spectra of silicate glasses compared to that of the aluminosilicate glasses analyzed in Le Losq et al. (2012). The OH stretch signal below 3000 $cm^{-1}$ in silicate glasses is intense and cannot be neglected, as Le Losq et al. (2012) did for aluminosilicate glasses. We modified the baseline definition accordingly, as shown in Figure S1. The corrected spectra were normalized to their total area between 350 and 4000 $cm^{-1}$. The area $A_w$ under the OH-stretching signal between 2000 and 4000 $cm^{-1}$ was measured (Figure S1). Such measurement on area-normalized spectra is equivalent to measuring the ratio between the area of silicate bands and that of the OH stretch band on non-normalized spectra. The water concentrations in NS4 glasses determined through FTIR analysis have been used to standardize the $A_w$ vs. total water concentration relationship. The remaining question was whether Raman cross-sections of the different OH signals observed near 3600, 2800, and even 2300 $cm^{-1}$, in silicate glasses (Figure S1) are equal. The cross-section of the Raman signals from individual species in the 3000-4000 $cm^{-1}$ range is independent of glass chemistry (Le Losq et al., 2012). The good agreement between the Raman-measured water concentrations, the nominal ones, and those determined by Loss On Ignition (Table 2) indicates that the O-H stretching Raman cross-section is not significantly dependent on the type of alkali element present in the glass. We conclude, therefore, that the OH stretching Raman cross-sections are not affected by the glass chemical composition. This maybe results from the fact that the OH stretching frequency is mostly controlled by one parameter, the O···O distances, and in agreement the OH stretching

638 Raman cross-section at a given frequency must mostly depend on this parameter in silicate
639 materials. The values in Table 2 are affected by a global error estimated from deviations
640 between the NS4 FTIR and Raman values and from numerical errors inherent to the baseline
641 subtraction and the calculation of OH stretching band area. Because we do not have a large
642 quantity of standards for performing the calibration and refining the standard deviation of the
643 technic, we preferred providing an error representing an upper limit, and equal to 0.30 wt% at
644 the 2σ confidence interval.
645

Table 1: Chemical composition of LS4, NS4 and KS4 anhydrous glasses. nom. mol%, nom. wt% and meas. wt% refer respectively to the nominal compositions in mol and wt%, and to the measured composition in wt%. Chemical analysis were conducted with a JEOL FE-SEM equipped with an energy dispersive spectrometer (EDS), and were acquired on 25 x 25 microns areas, with a 15 kV and 1.04 nA current. Errors are given at the σ confidence interval. **Lithium has been determined by difference.*

| | | **$SiO_2$** | **$Li_2O$*** | **$Na_2O$** | **$K_2O$** |
|---|---|---|---|---|---|
| **LS4** | nom. mol% | 80.00 | 20.00 | 0.00 | 0.00 |
| | nom. wt% | 88.94 | 11.08 | 0.00 | 0.00 |
| | meas. wt% | 88.77(94) | 11.23(75) | *n.a.* | *n.a.* |
| **NS4** | nom. mol% | 80.0 | 20.0 | 0.00 | 0.00 |
| | nom. wt% | 79.50 | 0.00 | 20.50 | 0.00 |
| | meas. wt% | 80.38(36) | *n.a.* | 19.62(31) | *n.a.* |
| **KS4** | nom. mol% | 80.0 | 20.0 | 0.0 | 0.0 |
| | nom. wt% | 71.84 | 0.00 | 0.00 | 28.16 |
| | meas. wt% | 71.16(49) | *n.a.* | *n.a.* | 28.84(28) |

653 Table 2: Water concentration in the glasses in mol% and wt%. Nom.: nominal water
654 concentration. Raman values are given by the calibration determined with the help of the NS4
655 FTIR water concentrations (Appendix 1). LOI: Loss on ignition (see discussion about them in
656 text). Errors from the Raman-based analyses include the calibration error determined on NS4
657 glasses and the errors resulting from area determination. Errors are given at the 2σ confidence
658 interval.
659

| Glass | nom. mol% $H_2O$ | nom. wt% $H_2O$ | T° of synthesis (°C) | Pressure (GPa) | Wt% $H_2O$ FTIR | Wt% $H_2O$ RAMAN | Wt% $H_2O$ LOI |
|---|---|---|---|---|---|---|---|
| | 3.28 | 1.12 | 1650 | 1.5 | - | 1.05(30) | 1.45(53) |
| **LS4** | 9.40 | 3.35 | 1650 | 1.5 | - | 3.61(30) | 3.08(22) |
| | 17.64 | 6.67 | 1650 | 1.5 | - | 7.15(30) | 6.89(7) |
| | 3.28 | 1.00 | 1450 | 1.5 | 1.21(12) | 1.05(30) | - |
| **NS4** | 9.40 | 3.00 | 1450 | 1.5 | 2.89(18) | 3.02(30) | - |
| | 17.64 | 6.00 | 1450 | 1.5 | 6.02(29) | 5.96(30) | - |
| | 3.28 | 0.90 | 1550 | 1.5 | | 1.10(30) | - |
| **KS4** | 9.40 | 2.71 | 1550 | 1.5 | - | 2.78(30) | - |
| | 17.64 | 5.44 | 1550 | 1.5 | - | 4.85(30) | - |

660

661 Table 3: Explained fraction of variances as a function of the number of components from the
662 PCA analysis of data.

| Component n° | Fraction of variance |
|---|---|
| 1 | 0.59232 |
| 2 | 0.98046 |
| 3 | 0.98984 |
| 4 | 0.99641 |
| 5 | 0.99853 |
| 6 | 0.99967 |
| 7 | 0.99990 |
| 8 | 1.00000 |

663

664 Figure 1: $^{1}$H MAS NMR spectra of LS4 (top), NS4 (middle), and KS4 (bottom) glasses with
665 3.3, 9.4 and 17.6 mol% water. Intensities are normalized to the total area of spectra and to the
666 water concentrations.
667
668 Figure 2: The low frequency spinning side bands $^{1}$H MAS NMR spectra of the LS4, NS4 and
669 KS4 glasses. One observes relatively strong side bands for Li, less strong for Na, and very
670 weak for K. $^{1}$H-$^{1}$H dipolar coupling mostly controls the side band intensity. In general, such
671 dipolar coupling is greatest for $H_2O^{mol}$ and would be non-existent for isolated $OH^-$ species.
672
673 Figure 3: Relative proportion of $H^+$ in the low-frequency LF (dark, signals < 1.8 ppm, see the
674 example $^{1}$H NMR spectrum in the insert), the middle-frequency MF (blue, between 1.8 and
675 7.7 ppm) and the high-frequency HF (red, signals > 7.7 ppm) spectral regions as a function of
676 the ionic radius of alkali ions (ionic radius values for a six-fold coordination from Whittaker
677 and Muntus, 1970). 3, 9 and 17 values are the mol% water concentrations of glasses truncated
678 of their decimal values.
679
680 Figure 4: Representation of the LS4, NS4, KS4 + 17.6 mol% $H_2O$ $^{1}$H spectra as a function of
681 the O-O distances, obtained by converting from the ppm scale with the equation from Eckert
682 et al. (1988). The square, diamond, star, hexagon and circle markers are visual markers of the
683 five environments of $H^+$. The legend at the bottom right summarizes the assignments
684 discussed in the text. ··· represents hydrogen bonds (HB). Intratet. HB refers to intratetrahedral
685 hydrogen bonding. BO is for bridging oxygen (Si-O-Si bonds). O(M)Si and O(H)Si represent
686 non bridging oxygen atoms involved in Si-O-M or Si-O-H bonds respectively; such notation
687 is adopted for clarity purpose.

688

689 Figure 5: Variation of the mean volume of the $H^+$ oxygen coordination sphere calculated from
690 $^1H$ MAS NMR spectra (see text), and of the partial molar volume $Vm_{H2O}$ of water at 1100°C
691 determined from solubility measurements (Mysen and Armstrong, 2002; Mysen and Cody,
692 2004). Error bars represent the standard deviation of the values calculated at different water
693 concentrations.

694

695

696 Figure S1: Raman spectra of the NS4 + 17.6 mol% $H_2O$ glass. A) Raw spectrum (dark) with
697 the spline cubic baseline (blue) constrained at 1400, 2000 and 3900 $cm^{-1}$; B) Baseline-
698 subtracted spectrum. Peaks at ~490 and ~1100 results from intertetrahedral bending and
699 intratetrahedral stretching of $SiO_4$ units respectively, while the ~800 $cm^{-1}$ band results from
700 $SiO_4$ rocking motions. The sharp band near 1630 $cm^{-1}$ results from $H_2O_{mol}$ bending, and the
701 2300, 2800 and 3600 $cm^{-1}$ bands results from OH stretching in OH and $H_2O_{mol}$ units in the
702 glass (Zotov and Keppler, 1998). See also Le Losq et al. (2012), Le Losq et al. (2014) and
703 references therein for details on Raman spectra of anhydrous and hydrous glasses. The
704 spectrum presented in B) is used for measuring the area of the signal assigned to OH
705 stretching (in red). Intensities of the spectrum have been previously normalized to the total
706 area of the spectrum, which is now equal to 1 (theoretical value of the sum of the vibrational
707 density of state).

708

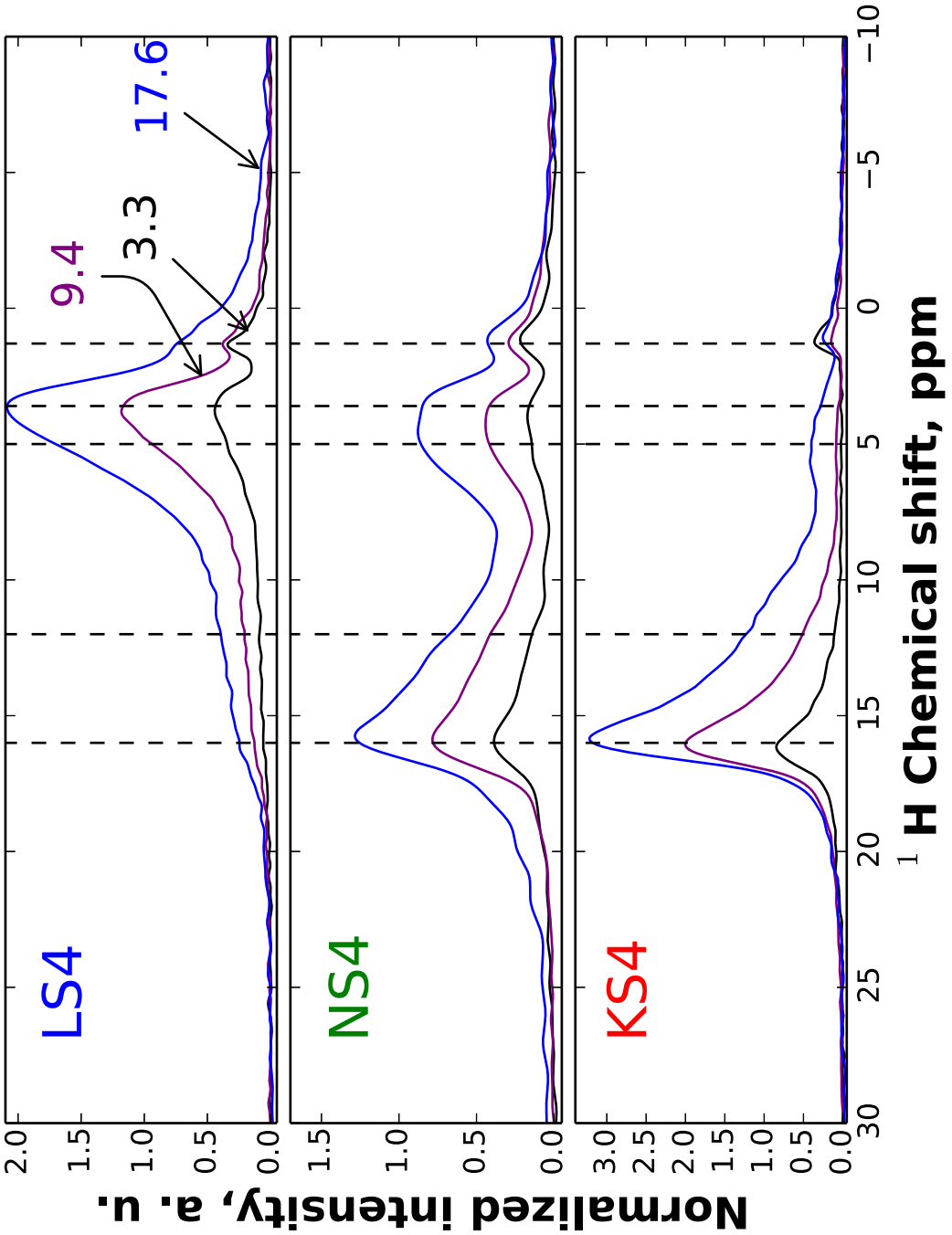
LS4
NS4
KS4
17.6
3.3
9.4
Normalized intensity, a. u.
$^1$H Chemical shift, ppm
2.0
1.5
1.0
0.5
0.0
3.0
2.5
30
25
20
15
10
5
0
−5
−10

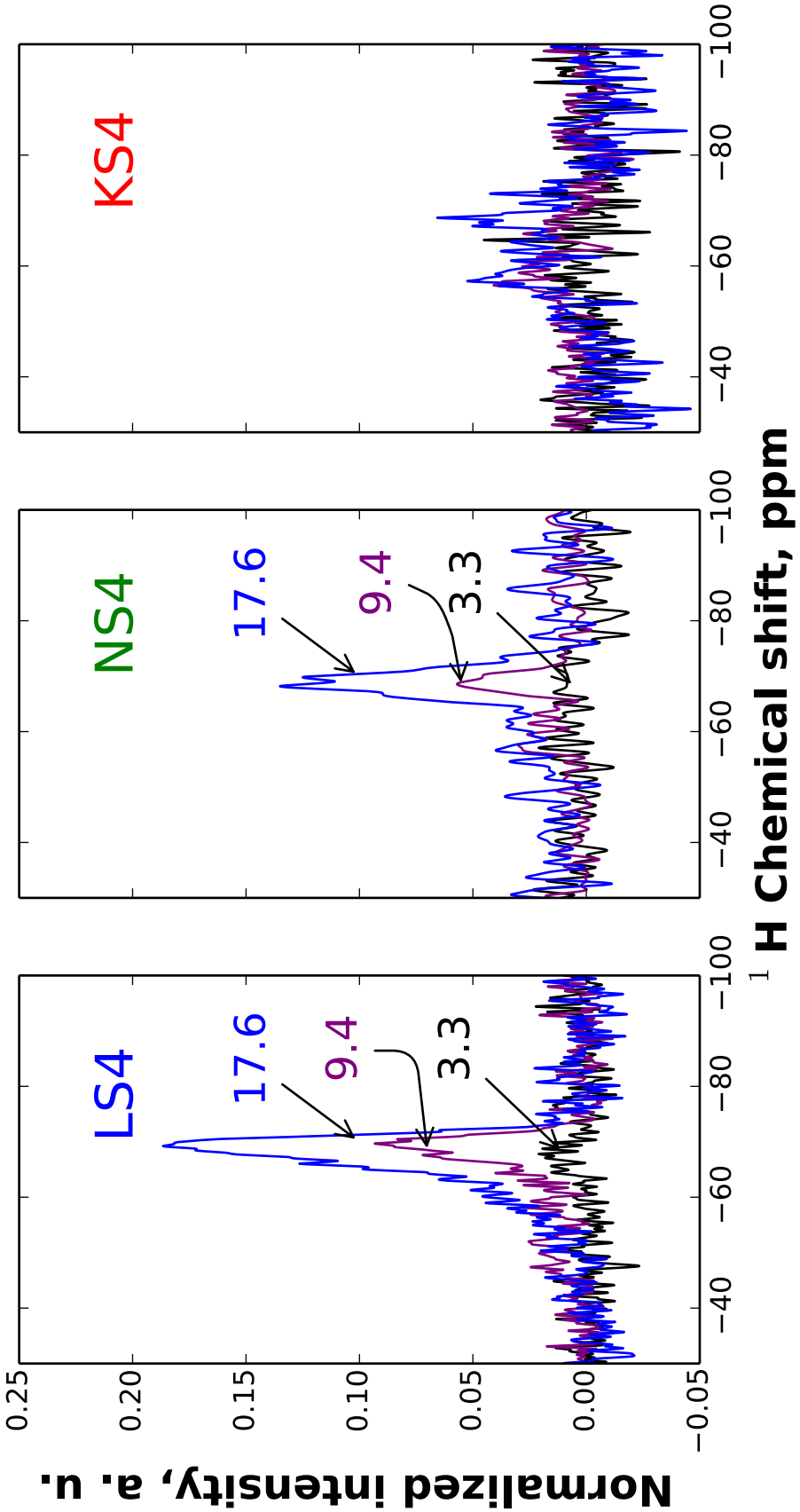
KS4
NS4
17.6
9.4
3.3
LS4
17.6
9.4
3.3
0.25
0.20
0.15
0.10
0.05
0.00
−0.05
−40
−60
−80
−100
Normalized intensity, a. u.
$^1$H Chemical shift, ppm

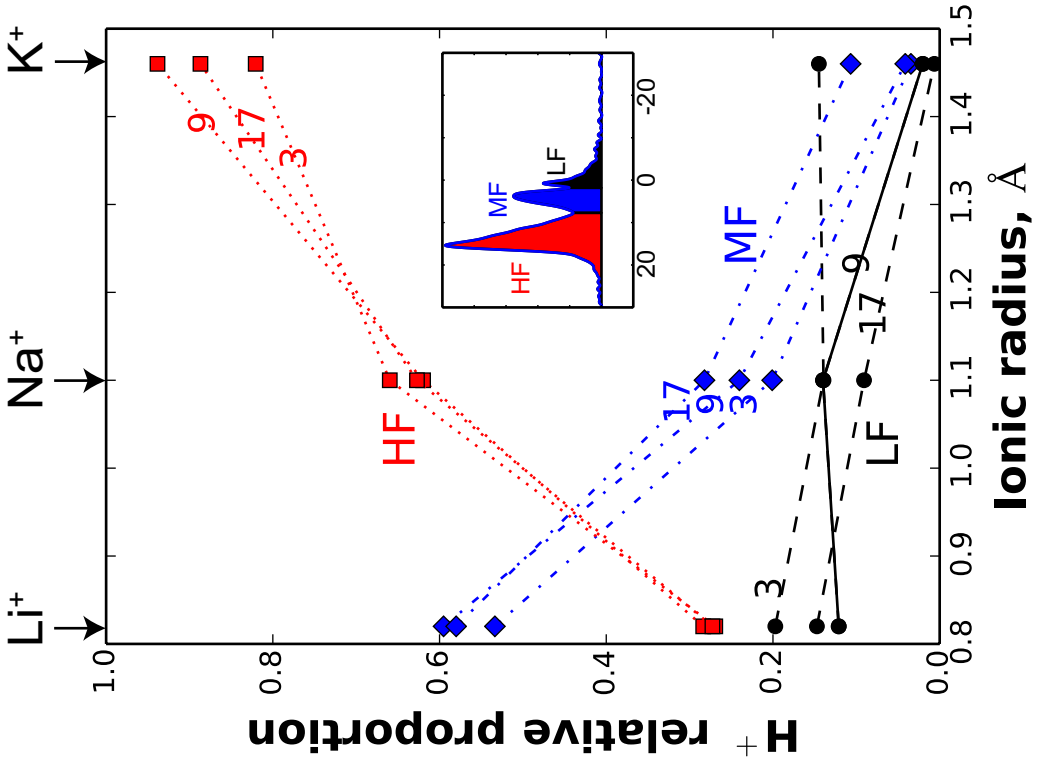
Li+
Na+
K+
H+ relative proportion
Ionic radius, Å
HF
MF
LF
9
17
3
20
0
-20

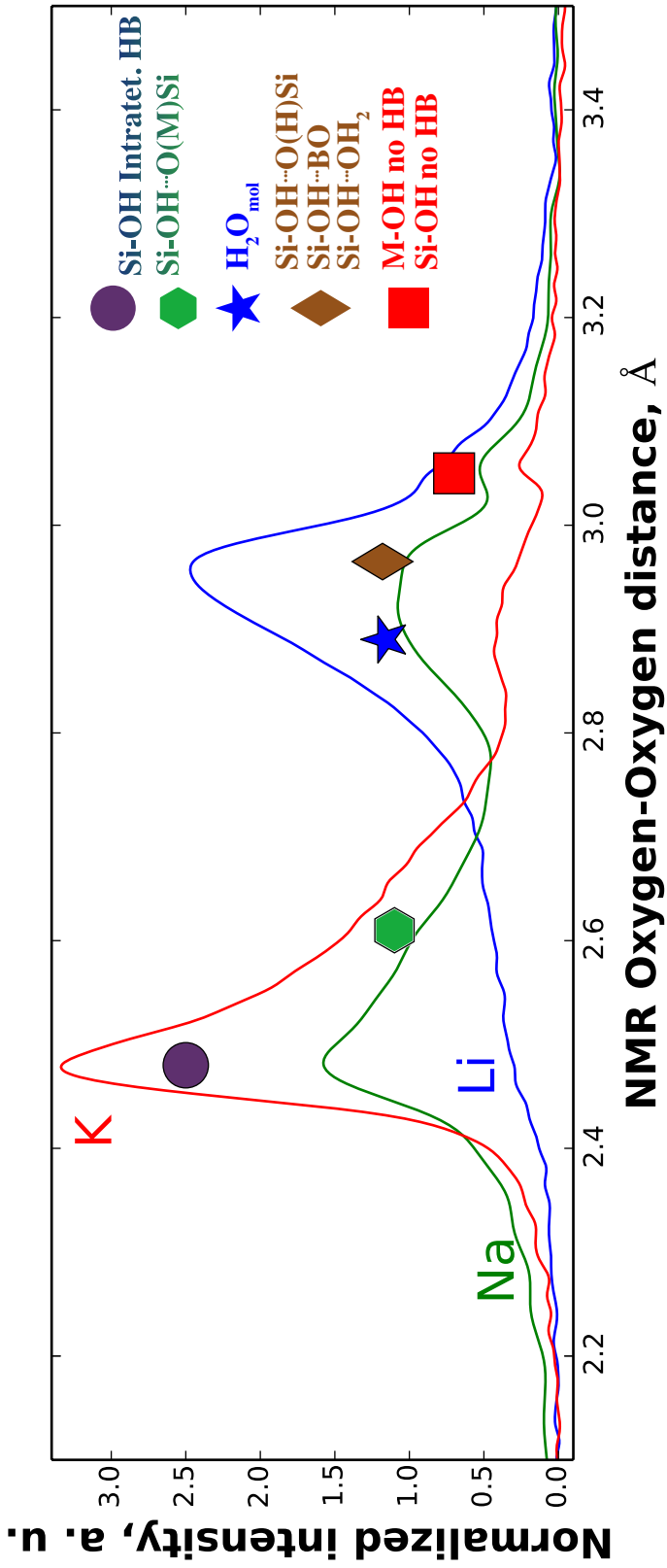
Normalized intensity, a. u.
NMR Oxygen-Oxygen distance, Å
0.0
0.5
1.0
1.5
2.0
2.5
3.0
2.2
2.4
2.6
2.8
3.0
3.2
3.4
K
Li
Na
Si-OH Intratet. HB
Si-OH···O(M)Si
H2Omol
Si-OH···O(H)Si
Si-OH···BO
Si-OH···OH2
M-OH no HB
Si-OH no HB

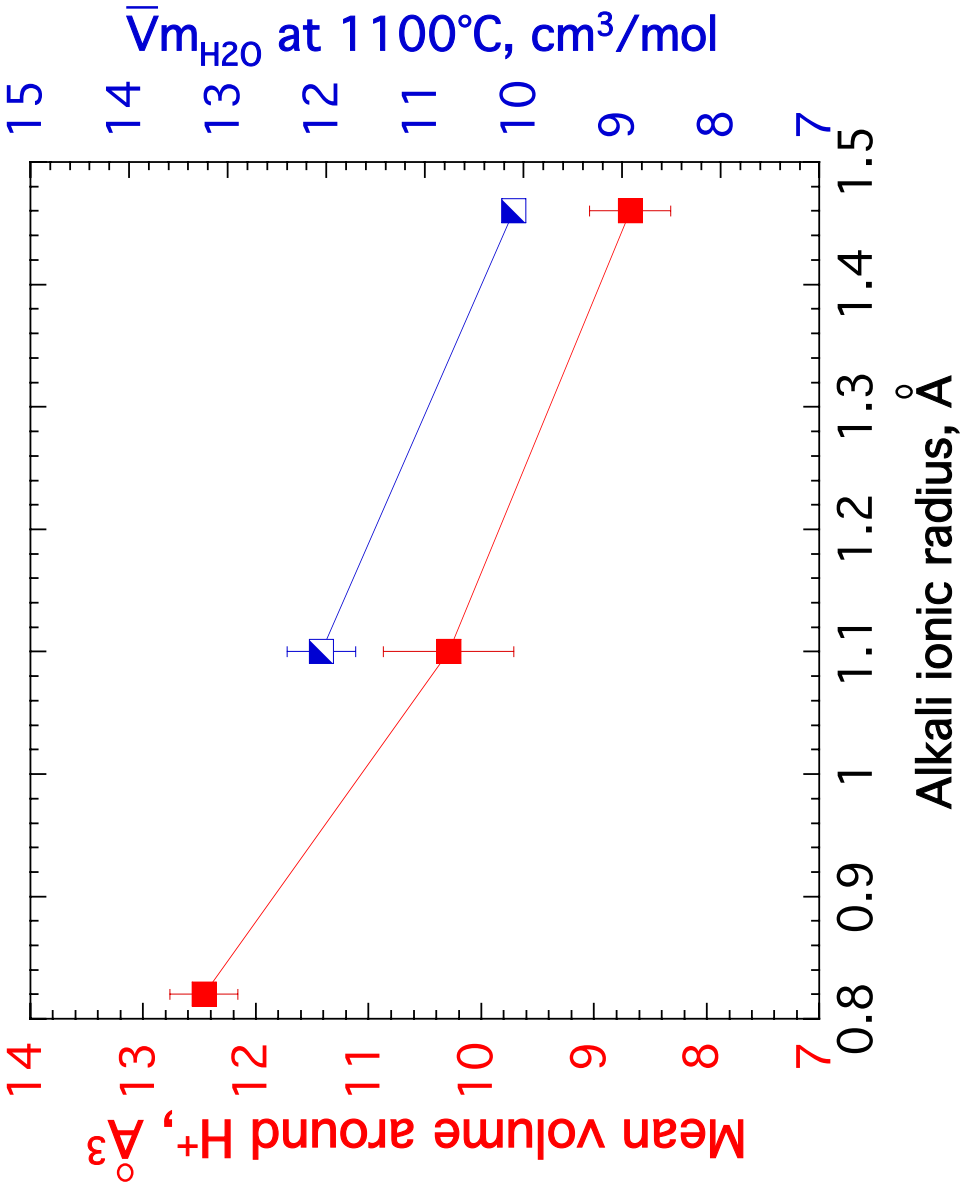
$\bar{V}m_{H2O}$ at 1100°C, cm³/mol
15
14
13
12
11
10
9
8
7
Alkali ionic radius, Å
0.8
0.9
1
1.1
1.2
1.3
1.4
1.5
Mean volume around H+, Å³
14
13
12
11
10
9
8
7